

# Glancing angle sputter deposited nanostructures on rotating substrates: Experiments and simulations

C. Patzig,<sup>1,a)</sup> T. Karabacak,<sup>2</sup> B. Fuhrmann,<sup>3</sup> and B. Rauschenbach<sup>1,4</sup>

<sup>1</sup>Leibniz-Institut für Oberflächenmodifizierung (IOM), Permoserstraße 15, D-04318 Leipzig, Germany

<sup>2</sup>University of Arkansas at Little Rock, 2801 South University Avenue, Little Rock, Arkansas 72204, USA

<sup>3</sup>Interdisziplinäres Zentrum für Materialwissenschaften (IZM), Martin-Luther-Universität Halle-

Wittenberg, Heinrich-Damerow-Straße 4, D-06120 Halle, Germany

<sup>4</sup>Institut für Experimentelle Physik II, Universität Leipzig, D-04308 Leipzig, Germany

(Received 16 July 2008; accepted 24 September 2008; published online 14 November 2008)

Ordered arrays of Si nanorods and nanospirals have been produced by ion beam sputter glancing angle deposition of Si on rotating substrates. The substrates were prepatterned with honeycomb and hexagonal-closed-packed arranged Au dots obtained by nanosphere lithography. The effects of template type, substrate rotational speed, height of the artificial Au seeds, and deposition angle  $\theta$  of the incident flux on the growth of the Si nanostructures is examined. Especially for the deposition of Si on honeycomb templates at different deposition angles, it is shown that the structure of the growing film changes drastically. A continuous film with honeycomblike arranged hillocks on top is deposited at normal incidence. With increased  $\theta$ , the structure shifts to almost dense films with a mesh of hexagonally arranged pores ( $\theta=70^\circ$ ). Finally, separated rodlike structures with triangular cross section are obtained under glancing angle conditions ( $\theta=85^\circ$ ). In addition, the structural evolution of the glancing angle deposited Si films is compared with oblique angle deposition three-dimensional Monte Carlo simulations. Furthermore, the effects of surface diffusion on the growth of spiral Si nanostructures on nontemplated substrates in experiment and simulation are compared and discussed. © 2008 American Institute of Physics. [DOI: 10.1063/1.3018145]

## I. INTRODUCTION

In recent years, the possibility to grow nearly arbitrary shaped nanostructures by oblique incidence deposition under controlled substrate rotation in a process commonly known as glancing angle deposition (GLAD)<sup>1,2</sup> has gained significant attention due to a manifold of possible applications, such as photonic crystals,<sup>3</sup> polarizing filters,<sup>4</sup> humidity sensors,<sup>5</sup> or pressure sensors,<sup>6</sup> to name only a few. If GLAD is performed on patterned substrates, the patterned mounds can serve as nucleation sites for the incoming particle flux and can shadow the area between those mounds, depending on the ratio of their height to the interseed distances. This will result in nanostructures grown on determined places with distinct periodicities. So far, most researchers have focused on tetragonal arrangements<sup>3,7–12</sup> or on hexagonal-closed-packed (hcp) arranged seeds consisting of self-assembled monolayers of nanospheres,<sup>13–15</sup> whereas only a few reports concerning the use of honeycomblike templates for GLAD exist<sup>16,17</sup> [the term “honeycomblike” is used to describe the hexagonal template pattern reminding of a honeycomb structure, as shown in Fig. 1(a), which is different from the hcp arrangement as shown in Fig. 1(b)]. Additionally, GLAD has been simulated mainly with Monte Carlo simulation codes to predict the development of obliquely deposited structures.<sup>9,18–20</sup>

However, if those simulations include substrate rotation, they mainly focus on the case of a sufficiently fast substrate

rotation, which results in the formation of rodlike structures. Only few researchers have so far reported on the simulation of GLAD on seeded substrates, and in those cases the seeds were arranged in simple tetragonal arrangements.<sup>9,20</sup> The influence of different rotational speeds on the development of glancing angle deposited nanostructures, especially on patterned substrates with more complex template geometries, has not been investigated in simulations so far, though. Also, most simulations and experiments deal only with the extreme cases of GLAD or normal incidence.

In this work, we will first discuss the influence of surface diffusion effects mediated by the substrate temperature  $T_S$  on the growth of Si nanospirals on nontemplated planar substrates in both experiment and simulation (Sec. IV A). Most experimental research in the field of GLAD so far has been done without elevated  $T_S$  values, arguing that if  $T_S$  exceeds approximately 0.3 times the melting temperature of the used material, the surface diffusion would counteract the desired self-shadowing effect in the deposition.<sup>21</sup> While some work

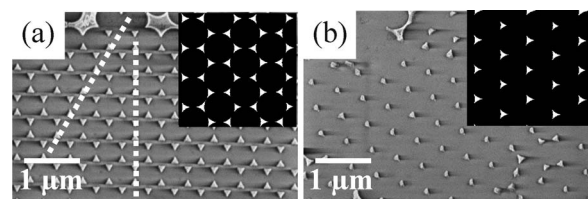


FIG. 1. Micrographs of the honeycomb (a) and hcp (b) templates used. The insets show the respective templates for the simulations. Dotted lines in (a): cut directions for growth exponent evaluation.  $d_1$ : equidistant seeds (left dotted line),  $d_2$ : seeds with alternating distances (right dotted line).

<sup>a)</sup>Author to whom correspondence should be addressed. Electronic mail: christian.patzig@iom-leipzig.de.

has been done on the temperature effect on the growth of Ta nanopillars on rapidly rotating substrates patterned with self-assembled SiO<sub>2</sub> nanospheres,<sup>13,14,17</sup> it has been shown that on stationary substrates unusual effects can occur with increased  $T_S$ , such as the growth of Al whiskers in a process called high temperature GLAD.<sup>22</sup> Additionally,  $T_S$  has been found to influence the merging behavior and structure diameter in the growth of Si nanostructures on rotating patterned substrates with slow and fast substrate rotation.<sup>23</sup> Simulations of GLAD including substrate diffusion effects usually concentrate on fast rotating substrates<sup>19,24</sup> or stationary substrates.<sup>25</sup> In contrast to that, the more complex case of an intermediate substrate rotational speed with different diffusion strengths in direct comparison of experiment and simulation will be shown here.

In the following sections, template patterns with two different geometries, either honeycomblike or hcp-like, will be introduced to deposit periodically arranged Si nanostructures by glancing angle sputter deposition both experimentally and in simulations. As described in a previous work,<sup>16</sup> the shape of the cross section of nanocolumns grown on prepatterned, rapidly rotating substrates with sufficiently large seed heights depends on the type of the template pattern used. To punctuate this finding, in Sec. IV B the influence of the template on the evolution of the growing structures will be briefly investigated both in experiment and simulation. In the following subsections, the focus will lie on the less symmetric honeycomb template pattern, as only little experimental work,<sup>16,17</sup> and to date no simulation work (to the authors' knowledge) has been reported on the combination of GLAD with this kind of template pattern.

## II. EXPERIMENTS

The surface patterning of the substrates was done by means of nanosphere lithography (NSL) as described in a previous work.<sup>26</sup> After patterning Si (100) substrates with monolayers and double layers of polystyrene (PS) nanospheres (sphere diameter  $s=419$  nm), Au was deposited through the pores between the spheres by thermal evaporation in high vacuum with nominal Au film heights of  $h(\text{Au})=5$  nm and  $h(\text{Au})=50$  nm. After the removal of the nanospheres, periodically arranged Au dots in honeycomblike (for the case of the nanosphere monolayers) or hcp (for the case of the nanosphere doublelayers) symmetry with nearest-neighbor distances of approximately 240 nm (honeycomb arrangement) or 420 nm (hcp arrangement) were obtained and used as artificial seeds for the subsequent GLAD growth of the Si nanorods. Micrographs of those templates can be seen in Figs. 1(a) and 1(b).

All GLAD experiments took place in an arrangement as described in previous articles<sup>11,12,27</sup> in a load-locked high vacuum chamber with a base pressure better than  $1.0 \times 10^{-8}$  mbar. Ar<sup>+</sup> ions extracted out of an inductively coupled, high frequency (13.56 MHz) ion source with a triple grid system (40 mm in diameter) were used to sputter the surface of a sintered Si disk (150 mm in diameter). An argon flux  $f_{\text{Ar}}=4.2$  SCCM (SCCM denotes standard cubic centimeter per minute at ATP) resulted in a working pressure

of  $p_{\text{dep}} \approx 8.3 \times 10^{-5}$  mbar while deposition. The substrates were attached to a substrate holder with continuously variable substrate tilt  $\theta$  (i.e., the angle between substrate normal and target normal), which is capable of a computer-driven substrate rotation around the substrate normal with rotational speeds  $\omega$  ranging between  $0.01 \text{ rpm} \leq \omega \leq 0.2 \text{ rpm}$ . A Ta wire resistance heater at the back side of the substrate holder was used to heat the samples during deposition, and a type K thermocouple at the back side of the substrate holder provided control over the substrate temperature  $T_S$  in a range between room temperature (RT) and  $T_S \approx 300$  °C. The ion source-target distance measured 15 cm, the target-substrate distance measured 12 cm, and the Ar<sup>+</sup> ion flux reached the target under an angle  $\phi_{\text{target}} \approx 65^\circ$  to the target normal. All experiments were done with an ion energy of 1100 eV. For different deposition angles  $\theta=0^\circ, 35^\circ, 70^\circ$ , and  $85^\circ$ , the film deposition rates at  $T_S=\text{RT}$  amounted to  $r=21.5 \pm 1.0$ ,  $17.3 \pm 0.5$ ,  $9.6 \pm 0.3$ , and  $5.3 \pm 0.2$  nm/min. For otherwise constant deposition parameters, the ratio of vertical deposition rate to rotational speed ( $\rho=r/\omega$ ) could be adjusted by changing  $\omega$ .

After growth, the samples were cleaved and examined with scanning electron microscopy (SEM) at 2.5 kV acceleration voltage and 5 mm working distance. The analysis of the micrographs was done using the commercially available scanning probe image processor<sup>28</sup> version 3.2.6.0. with the grain detection module.

## III. SIMULATIONS

A three-dimensional (3D) Monte Carlo method was used to simulate and investigate the growth of GLAD nanostructures on flat and patterned substrates.<sup>19,24,29</sup> A square lattice with continuous boundary conditions was formed by cubic lattice points and each incident atom has the dimension of one lattice point. The simulations included an obliquely incident flux, substrate rotation, and surface diffusion. In order to model the angular distribution in a typical sputter deposition, the incident flux had an angular spread (centered around the incident beam) according to the distribution function  $dP(\theta, \phi)/d\Omega = (2 \cos \theta)/(\pi \sin \theta)$ , where  $\theta$  is the polar angle and  $\phi$  is the azimuthal angle.<sup>18</sup> In the simulations, it was assumed that the particle energies are negligible, and hence no momentum transfer takes place when particles land on the surfaces. At each simulation step, an atom was sent towards a randomly chosen lattice point on the surface of size  $512 \times 512$  lattice units (lu). For GLAD simulations on patterned substrates, honeycomb and hcp templated substrates with various seed heights and different sphere diameters (in units of lu) were designed (it has to be mentioned that the simulated seeds have a flat top, different to the more pyramidal-shaped seeds used in the experiments). To take into account the substrate rotation, each atom was sent with a change in the azimuthal angle of  $\Delta\phi$  degrees from the previous one. Overhangs (sidewall sticking) on the surface were allowed during deposition that results in truly 3D structures. After the incident atom was deposited onto the surface, a surface or bulk atom within the vicinity of  $\pm 5$  lu of the impact point was chosen randomly to diffuse to another

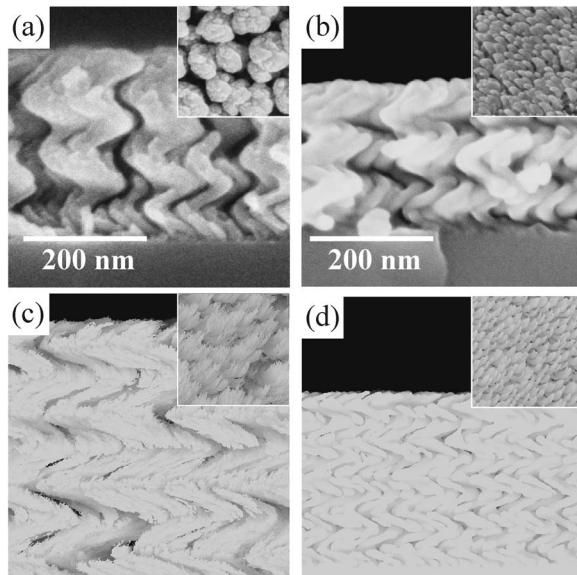


FIG. 2. Effect of diffusion on spiral-like structures: Si spirals deposited at (a)  $T_S = \text{RT}$  and (b)  $T_S = 300\text{ }^\circ\text{C}$  at the same deposition time. MC simulations of glancing angle sputter deposited spirals with number of diffusion steps (c)  $D = 10$  and (d)  $D = 300$  for the same number of simulated particles. Insets: corresponding top views.

nearest-neighbor random location. The probability of this diffusion was related to how many nearest neighbors the particle has before hopping. When the particle has lots of nearest neighbors, the probability of hopping gets less. The diffusion step was repeated until the assigned number of jumps ( $D$ ) is made. Then another atom was sent and the deposition and diffusion steps are repeated in a similar way. Our simulations were conducted for different values of deposition angles  $\theta$ , surface diffusion hops  $D$ , and on flat and patterned substrates. Other variables also included total number of particles (NOP) sent throughout deposition and number of particles per rotation (NPR).

## IV. RESULTS AND DISCUSSIONS

### A. Nontemplated substrates: Effect of substrate temperature

When GLAD of Si is performed on rotating substrates, the ratio  $\rho = r/\omega$  determines the developing structure type.<sup>30</sup> If  $r$  is kept constant, an increase of  $\rho$  can be achieved by a decrease of  $\omega$ . Starting from low  $\rho$  values that would lead to the growth of vertical rodlike structures, decreasing  $\omega$  will induce a shift of the structure type from vertical nanorods over screwlike structures (compact core) to finally spiral-like structures (hollow core). For the ion beam sputter glancing angle ( $\theta = 85^\circ$ ) deposited Si nanostructures described here, it was found that at a substrate temperature  $T_S = \text{RT}$ , spirals are deposited if  $\rho > 120\text{ nm/rev}$  on flat substrates.<sup>23</sup> Figure 2 compares the effect of an enhanced surface diffusion on the morphological evolution of spiral GLAD structures in experiment and simulation. As shown in Fig. 2(a), at  $T_S = \text{RT}$  and  $\rho = 175\text{ nm/rev}$ , the growth process starts with the development of single spiral fibers with fiber diameters on the 30 nm range. As growth continues, those fibers eventually merge to form broader structures. With increasing  $T_S$ , how-

ever, the morphological evolution changes [see Fig. 2(b) at  $T_S = 300\text{ }^\circ\text{C}$ ], and the single spiral fibers show no merging and stay as separated nanospirals. The insets of the Figs. 2(a) and 2(b) show the respective top-view micrographs that also indicate the structural change from broad, merged structures at  $T_S = \text{RT}$  to separated nanospirals at  $T_S = 300\text{ }^\circ\text{C}$ . Additionally, a densification of those nanostructures can be observed with increasing  $T_S$ , as the film height decreases for the same deposition time and therefore same amount of deposited material (in the film as shown in Fig. 2, the film height  $t$  changes from  $t(\text{RT}) = 535\text{ nm}$  to  $t(300\text{ }^\circ\text{C}) = 405\text{ nm}$ , i.e., a decrease in film height of approximately 24%).

Simulating the influence of surface diffusion on the growth of spiral-like glancing angle deposited thin films effectively reflects the actual experimental results, as can be seen in Figs. 2(c) and 2(d). In this case, the following parameters were used:  $\theta = 85^\circ$ ,  $\text{NOP} = 5 \times 10^7$ , and  $\text{NPR} = 1 \times 10^7$ . The number of diffusion steps  $D$  changes from  $D = 10$  [Fig. 2(c)] to  $D = 300$  [Fig. 2(d)]. It is observable that similar morphological changes as seen in the experiment take place in the simulations. Low surface diffusion ( $D = 10$ ) leads to the growth of bundled structures, whereas high surface diffusion ( $D = 300$ ) fosters the growth of nanostructured thin films that consist of separated spirals with smaller diameters as compared to the low surface diffusion case. Just as in the experiment, the overall density of the simulated film decreases with increasing  $D$ , which is reflected in a decrease of film height of approximately 28% from  $D = 10$  to  $D = 300$  for otherwise constant simulation parameters.

The effects of film densification and delayed merging with increasing  $T_S$  for spiral-like nanostructures can be described as effects of enhanced surface diffusion and therefore increased mobility of the deposited Si particles.<sup>23</sup> An increased surface mobility of the adatoms that reach the tops of the spiral-like fibers that are already deposited enhances the probability of the incoming particles to diffuse along the sides of those fibers. Therefore, the broadening and merging of those fibers due to capturing and immobilization of the incoming flux is delayed. As a consequence, the fibers stay separated for a longer growth period without merging. The shown densification effect with increased  $T_S$  can be explained with surface diffusion as well. At low  $T_S$  (negligible surface diffusion), the incoming particles are unable to travel long distances along the fibers. Thus, the fiber diameter of the spiral-like structures gradually increases. Some of the single structures may gain more flux than their neighbored ones (for example, due to deviations in the incoming particle flux), exacerbating the self-shadowing effects of adjacent structures and finally leading to the extinction of some of the structures or to merging of single structures to broader entities. The surviving structures capture all the incoming particle flux, leading to films that consist of broad structures with large interstructure distances [as can be seen in Fig. 2(a)]. At higher  $T_S$ , however, the increased particle mobility fosters the growth of dense, separated spirals with equal structure diameters.

The performed simulations with  $D = 10$  and  $D = 300$  diffusion steps support the assumption of a surface diffusion-driven structure change of the grown nanostructures from

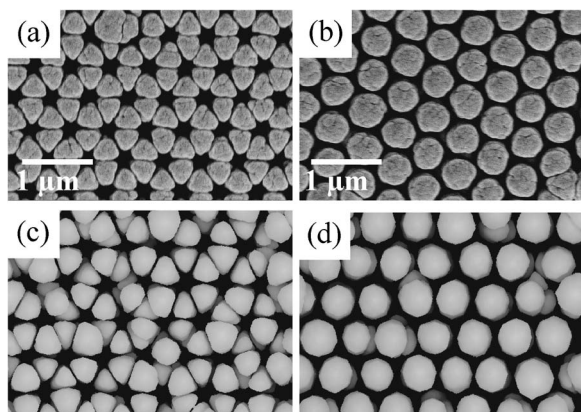


FIG. 3. Top-view micrographs of Si nanocolumns grown on honeycomb substrate with triangular cross section on honeycomb templates (a) and with circular cross section on hcp templates (b). Top views of simulations of glancing angle deposited nanocolumns run on honeycomb (c) and hcp (d) template.

broad, merged structures to a film of densely packed, smooth spirals with equal diameters. Although the resemblance between the experiments at  $T=RT$  and the simulations at  $D=10$  diffusion steps [Figs. 2(a) and 2(c)] is not as clear as in the high temperature case [Figs. 2(b) and 2(d)], the same trends concerning film densification and development of isolated, spiral-like structures with increased substrate temperature (i.e., surface diffusion) are observable in both experiments and simulations. Figure 2 shows a transition from a film consisting of hardly distinguishable, broad, spiral-like structures with rugged surface features [ $D=10$ , Fig. 2(c)] to a film that comprises clearly separated, densely packed spirals with smooth surfaces and equal diameters [ $D=300$ , Fig. 2(d)].

It has to be added, though, that this discussion only holds for a certain range of  $T_S$ . When  $T_S$  is increased to values greater than  $300\text{ }^\circ\text{C}$ , an early broadening of adjacent structures can be observed, which is attributed to the surface diffusion getting sufficiently large to overcome the distances between single spiral fibers right in the beginning of the growth process.<sup>23</sup> Additionally, it has to be pointed that in the following sections, concerning templated substrates  $D=300$  diffusion steps resembled the experimental results at  $T_S=RT$  better. Obviously, it is not possible to assign fixed  $D$  values to fixed  $T_S$  values in this simple model. However, to indicate the trends of structural changes with a change of substrate temperature, the used simulation model with two different diffusion steps, differing by one order of magnitude, fits well with the experimental results.

## B. Templated substrates: Influence of template pattern

Two different template geometries were used to grow vertical Si rods with nominal heights  $t=685\text{ nm}$  with a fast substrate rotation ( $\rho=26\text{ nm/rev}$ ) under glancing angle conditions ( $\theta=85^\circ$ ) on NSL patterned substrates with seed heights  $h(\text{Au})=50\text{ nm}$  and sphere diameter  $s=419\text{ nm}$ . Figures 3(a) and 3(b) show top-view micrographs of Si rods grown on those substrates. Evidently, as described in a previous article,<sup>16</sup> on honeycomblike arranged patterns the cross

sections of the structures evolve a triangular shape, whereas on the hcp pattern, the cross section of the structures is more circular.

In order to simulate the growth of oblique angle deposited thin films on templates with distinct honeycomb or hcp arrangement, template patterns with specific geometries and seed heights that resemble the experimental case of NSL-obtained templates were developed, as can be seen in the insets of Figs. 1(a) and 1(b). The simulations were run under the following parameter set:  $D=300$  diffusion steps, seed height  $h=15\text{ lu}$ ,  $\text{NPR}=1\times 10^6$  (fast substrate rotation), and  $\text{NOP}=1.5\times 10^7$ . Figures 3(c) and 3(d) show top views of the simulated films. Just as in the experiments, the evolution of periodically arranged structures with triangular shaped cross sections on honeycomb templates and with more circular cross sections on hcp templates can be observed.

Both experiments and simulations result in the same trends regarding the morphological development of glancing angle sputter deposited rodlike nanostructures on patterned substrates, indicating a sufficiently good compliance between the physical deposition mechanism and the model adapted for the simulations that involves an angular distribution function of the sputtered particle flux, diffusion by means of particle hopping, oblique angle deposition, and substrate rotation by changing the azimuthal angle of incoming particles sent to the substrate one by one.

Following the discussion in a previous work,<sup>16</sup> the different cross sections of the vertical Si rods that develop through glancing angle sputter deposition on either honeycomblike or hcp templated substrates are a consequence of the different template geometries. In the hcp case, each seed is surrounded by six equidistant neighbors. Therefore, it follows that on rapidly rotating substrates with the flux coming effectively from every direction toward the seeds,<sup>30</sup> the rod diameter will expand homogenously in every direction. As a consequence, rods with nearly circular cross sections develop during growth. Different from that on honeycomblike templated substrates, the seeds are not equidistantly distributed across the substrate surface. As indicated in Fig. 1(a), in different growth directions, the distances between adjacent seeds are different. As a consequence, while at a certain stage of deposition the lateral expansion of the structure in directions with closely adjoining seeds (“side walls” of the honeycomb structure) terminates, it still can grow in directions with seeds separated over longer distances (direction of the “center” of the honeycomb structure). This results in the triangular shape of the rods’ cross section and will be discussed in more detail in Sec. IV D.

## C. Honeycomb templated substrates: Influence of substrate rotation speed

As can be seen in Figs. 4(a), 4(c), and 4(e), the experiments performed at  $\theta=85^\circ$  and  $T_S=RT$  show that under GLAD conditions, the Au dots on the substrate serve as artificial seeds and get decorated by the incoming Si particles. With the height of the Au dots  $h(\text{Au})\approx 50\text{ nm}$ , the shadowing length  $l=h(\text{Au})\times \tan\theta\approx 570\text{ nm}$  is larger than the distance between two Au dots that are separated by the circular

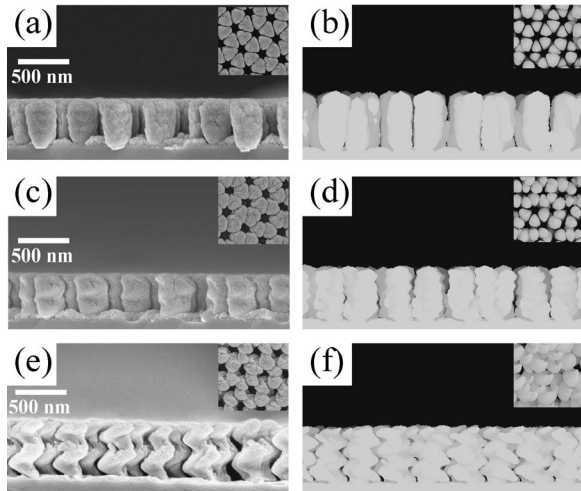


FIG. 4. Comparison of experimentally obtained and simulated nanostructures on honeycomb templates at different rotational speeds. Experiments were done at  $T_S=RT$  on honeycomb templates with a nominal height  $h(\text{Au})=50$  nm of the Au seeds and a PS sphere diameter  $s=419$  nm. Simulations were run at  $D=300$  with a seed height  $h=15$  lu and an according sphere diameter  $s=70$  lu. [(a) and (b)] Fast rotation ( $\rho=100$  nm/rev and  $\text{NPR}=1 \times 10^6$ ). [(c) and (d)] Intermediate rotational speed ( $\rho=180$  nm/rev,  $\text{NPR}=3 \times 10^6$ ). [(e) and (f)] Slow rotation ( $\rho=270$  nm/rev and  $\text{NPR}=5 \times 10^6$ ).

gap caused by the PS nanosphere with diameter  $s=419$  nm. Thus, the whole interseed region should be shadowed by the Au dots. The interseed growth that is clearly visible between the structures grown on the Au dots is therefore attributed to nondirectional flux that results from the sputtering technique used for the experiments. Just as in the case of the nontemplated substrates, an increase of the substrate rotation speed  $\rho$  induces a morphological change of the grown structures on the templated substrates from vertical rodlike over screwlike to spiral-like. However, the total values of  $\rho$  are different. In the case of the flat substrate, values of  $\rho > 120$  nm/rev lead to the growth of spiral-like Si structures.<sup>23</sup> On the honeycomb templated substrates, however, rodlike structures were grown with  $\rho=100$  nm/rev, screwlike structures evolved at  $\rho=180$  nm/rev, and spirals were deposited with  $\rho=270$  nm/rev on top of the Au dots.

A direct comparison of the experimental results with the MC simulated GLAD ( $\theta=85^\circ$ ) on honeycomb templates at different NPR values shows that comparable results are gained with the same trends, as can be seen in Fig. 4. The simulations show the evolution of broad, single structures that stuck to the lattice sites of the template and reproduce the templates periodicity, with low but recognizable interseed growth. Just as in the experiments, an increase of NPR ( $\text{NPR}=1 \times 10^6, 3 \times 10^6, 5 \times 10^6$ ) changes the structure morphology from rodlike to screwlike and spiral-like. The simulations were performed with a number of diffusion steps of  $D=300$ , which resembled best the experimental results at  $T_S=RT$  on honeycomb templates, with a PS nanosphere diameter  $s=70$  lu and seed heights  $h=15$  lu.

As described in the experimental part, increased  $\rho$  values as compared to the growth on nontemplated substrates are needed in order to gain spiral-like, screwlike, and rodlike structures on honeycomblike patterned substrates. This is a

result of the increased diameter of the structures grown on a templated substrate in comparison to structures grown on a flat substrate. Without template, the GLAD-grown structures typically evolve out of fibers with diameters in the 30 nm range that eventually merge together to form broader structures. As those fibers grow close together, the self-shadowing of neighbored structures prevents structure broadening. On templated substrates, however, the artificial seeds having a specific height and diameter serve as nucleation sites for the incoming particle flux. Thus, the incoming particle flux agglomerates on those seeds and evolves into nanostructures with saturated diameters that depend mainly on the interseed distances<sup>17</sup> and are usually at least one order of magnitude higher than in the case of the nontemplated substrate. In the described case of Si on honeycomb templated substrates with nanosphere diameters of  $s=419$  nm, the saturation diameter of the structures growing on the Au dots will be in the range of 250 nm for GLAD conditions ( $\theta \approx 85^\circ$ ). Under those circumstances, in order to keep the ratio of the pitch (that is, the height of the nanostructure after one full substrate revolution) to the structure diameter high enough to still be able to recognize the screwlike or spiral-like morphology,  $\rho$  has to be increased as compared to the template-free case.

Just as in the experiment, a change of in  $\rho$  induces a morphological shift from rodlike over screwlike to spiral-like structures, changing NPR in the simulations shifts the nanostructures morphologies in an equal manner. A fast rotation is resembled by low NPR values and resembles a unidirectional GLAD flux, thus leading to upright, rodlike structures. Increasing NPR leads to a particle flux that circularly rotates around the seeds on the substrate surface (as seen from the substrate). Therefore, screwlike or spiral-like structures whose ends “follow” the direction of the incoming flux will evolve. This morphological evolution is clearly seen in both simulation and experiment. Also, the ratios of the  $\rho$  and NPR values that result in different structure morphologies are of the same order of magnitude ( $\rho(\text{spiral})/\rho(\text{rod}) \approx 3$ ,  $\text{NPR}(\text{spiral})/\text{NPR}(\text{rod})=5$ ), indicating that the used simulation parameters are well suited to reflect the experimental results.

The interseed growth found in both experimental and simulation results is attributed to nondirectional flux due to the rather broad angular deposition of the sputtered particle flux. There appears to be less interseed growth in the simulations, which can be assigned to the different ratios of seed height  $h$  (Au) to sphere diameter  $s$ . In the experiments, this ratio is approximately  $50 \text{ nm}/419 \text{ nm}=0.12$ , whereas in the simulations, this ratio is  $15 \text{ lu}/70 \text{ lu}=0.21$ . Thus, more flux is captured by the seeds in the simulations as compared to the experiments, which results in less growth between the Au seeds on the substrate.

It has to be pointed out, however, that whereas in the case of a nontemplated substrate,  $D=10$  diffusion steps was suited best to simulate the growth at  $T_S=RT$ , in the case of a templated substrate  $D=300$  diffusion steps were found to resemble the experimental results better.

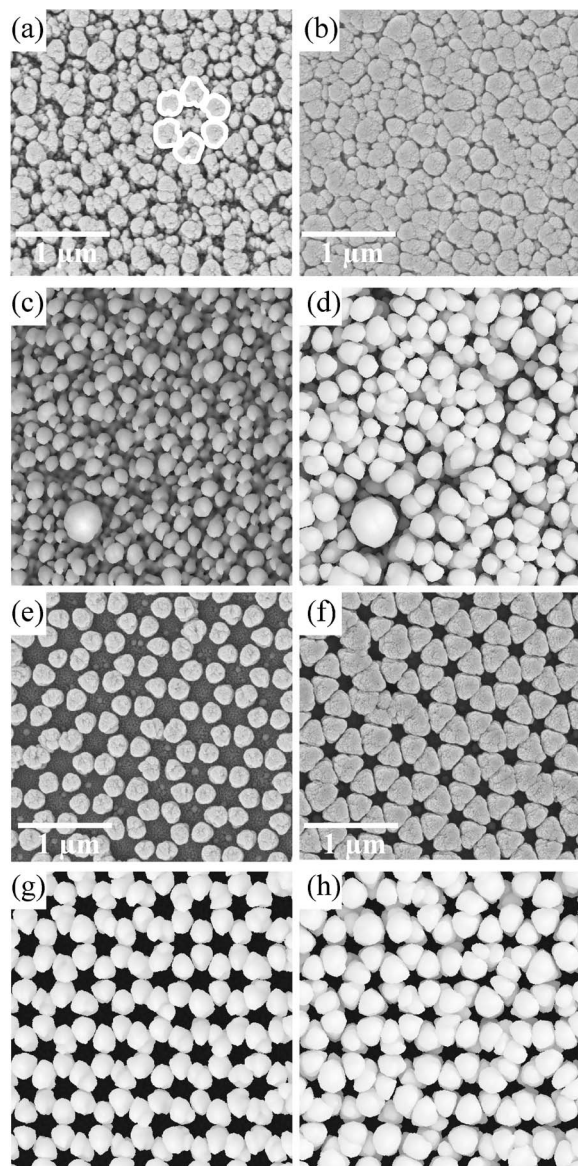


FIG. 5. Influence of different seed heights at different stages of growth. Experiments were done at  $T_S=RT$  on honeycomb templates with a PS sphere diameter  $s=419$  nm. Simulations were run at  $D=300$  with a sphere diameter  $s=70$  lu at  $NPR=3 \times 10^6$ . (a)  $h(\text{Au})=5$  nm,  $\rho=180$  nm/rev,  $t=320$  nm (exemplarily highlighted: six structures grown on honeycomblike arranged Au seeds). (b)  $h(\text{Au})=5$  nm,  $\rho=180$  nm/rev,  $t=430$  nm. (c)  $h=5$  lu,  $NOP=0.5 \times 10^7$ . (d)  $h=5$  lu,  $NOP=1.5 \times 10^7$ . (e)  $h(\text{Au})=50$  nm,  $\rho=100$  nm/rev,  $t=320$  nm. (f)  $h(\text{Au})=50$  nm,  $\rho=100$  nm/rev,  $t=430$  nm. (g)  $h=60$  lu,  $NOP=0.5 \times 10^7$ . (h)  $h=60$  lu,  $NOP=1.5 \times 10^7$ .

#### D. Honeycomb templated substrates: Influence of seed height

The influence of the seed height  $h$  (Au) on the evolution and regular arrangement of sputter deposited Si nanostructures is exemplarily shown for a honeycomblike arranged seed pattern (PS nanosphere diameter  $s=419$  nm) with two different seed heights  $h$  (Au) for the glancing angle case of  $\theta=85^\circ$  at  $T_S=RT$  for two different film heights  $t$ .

As can be seen in Figs. 5(a) and 5(b),  $h(\text{Au})=5$  nm (according to a shadowing length  $l \approx 57$  nm) is insufficient to shadow the whole region between neighbored seeds. Therefore, the lateral periodicity of the honeycomb pattern is not preserved, which results in a random nucleation and non-

periodically arranged structures. However, it is observable that in the beginning of growth [ $t=320$  nm, Fig. 5(a)], on the honeycomblike arranged Au seeds the growing structures are broader (one honeycomb pattern is highlighted in Fig. 5(a) to underline this point), with diameters being in the range of 150 nm, whereas in between the Au seeds, several smaller structures with diameters on the 50 nm range are grown. As the deposited structures grow larger [ $t=430$  nm, Fig. 5(b)], the diameters of the deposited nanostructures increase, leading to a densification of the whole film. If  $h$  (Au) is increased sufficiently in order to shadow the whole space between the seeds, almost the whole flux is captured by the Au seeds, resulting in honeycomblike periodically arranged nanostructures. In Figs. 5(e) and 5(f), two different stages of nanostructure growth are shown on seeds with  $h(\text{Au})=50$  nm ( $l \approx 570$  nm). Again, an increase of the structures diameters is clearly observable with increasing  $t$  from 320 to 430 nm. Additionally, it is worth noticing that the cross section of the growing nanostructures gradually evolves into a triangular shape, which will be discussed later.

The simulations were run with different seed heights of  $h=5$  lu and  $h=60$  lu, a sphere diameter  $s=70$  lu and a deposition angle  $\theta=85^\circ$  with  $NPR=3 \times 10^6$  and  $D=300$  diffusion steps. In order to show different stages of the simulated growth, top-view pictures of the simulations after  $NOP=0.5 \times 10^7$  and  $1.5 \times 10^7$  are shown in Fig. 5.

The results show that at  $h=5$  lu, no decoration of the seeds can be observed. The nucleation and subsequent nanostructure growth takes place at random locations on the surface. Just as in the experiment, a densification of the growing STF, caused by an increase of the structures diameters, can be found as well [Figs. 5(c) and 5(d)]. The simulations also show that increasing  $h$  leads to an almost complete shadowing of the interseed space, which in turn results in a decoration of the honeycomblike arranged seeds and the growth of periodically arranged nanostructures [Figs. 5(g) and 5(h)]. Comparable to the experimental finding, in the case of a sufficiently large seed height  $h$ , the increase in the film thickness  $t$  does not only lead to an increase in the structure diameter, but also to the development of a triangular cross section of the growing nanostructures.

Both experiments and simulations clearly indicate two trends observable in the GLAD of nanostructures on patterned substrates. Obviously, in order to gain a periodic arrangement of nanostructures that grow on the artificially provided seeding spaces, the height of those seeds must be sufficient enough to shadow the whole interseed spacing.

Additionally, an increase of structure diameter with increasing structure height as often described in other publications<sup>9,19</sup> is found in both experiments and simulations, regardless of the seed height. However, as can be seen when comparing Figs. 5(a) and 5(c), differences between experiments and simulations occur regarding the growth on templated substrates with seed heights that are insufficient to shadow the whole interseed region. As highlighted in Fig. 5(a) ( $t=320$  nm), the honeycomb-arranged Au seeds capture sufficient incoming particles to develop into broad, single structures that are intersected by numerous structures with smaller diameters growing off smaller nuclei that form in

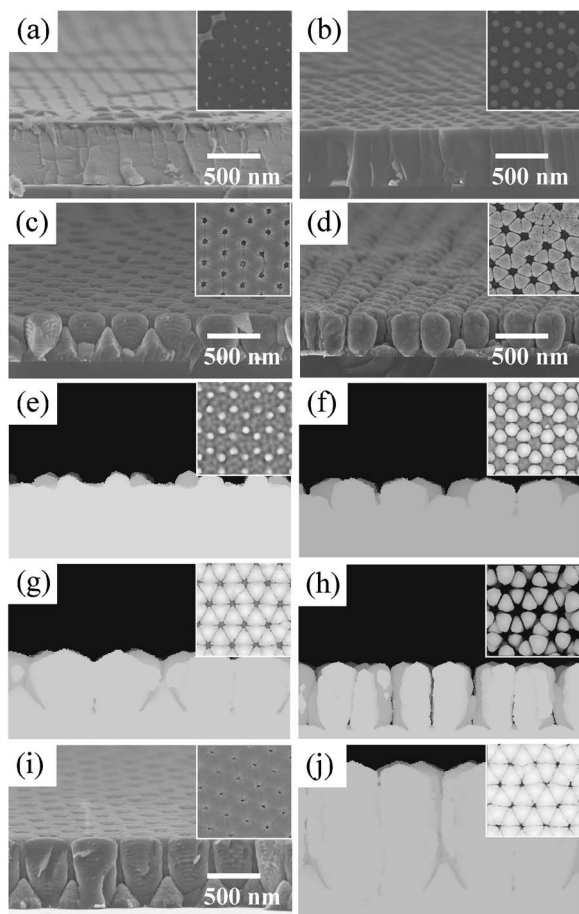


FIG. 6. Influence of the incoming angle  $\theta$  on the morphology of GLAD-grown nanostructures. Experiments were performed at  $T_S=RT$  with  $\rho \leq 105$  nm/rev, with adjusted deposition time to gain comparable film heights  $430 \text{ nm} \leq t \leq 490$  nm, on honeycomb templates with  $s=419$  nm and  $h(\text{Au})=50$  nm. Simulations were run on honeycomb templates with  $s=70$  lu at  $\text{NPR}=1 \times 10^6$  and  $\text{NOP}=1.5 \times 10^7$ , with  $h=15$  lu. [(a)–(d)]  $5^\circ$ -tilted cross sectional micrographs of Si films deposited at  $\theta=0^\circ$ ,  $35^\circ$ ,  $70^\circ$ , and  $85^\circ$ . [(e)–(h)] Simulated films for deposition angles  $\theta=0^\circ$ ,  $35^\circ$ ,  $70^\circ$ , and  $85^\circ$ . (i) Film deposited at  $\theta=70^\circ$  with  $t=670$  nm. (j) Simulated film at  $\theta=70^\circ$  with  $\text{NOP}=3 \times 10^7$ . The insets show the corresponding top views.

between the artificial seeds due to the insufficient shadowing mechanism as described above. The simulation in Fig. 5(c) does not show a preferred nucleation at the seeds, although the shadowing mechanism should be more efficient here as compared to the experiment, since the ratio of seed height to sphere diameter in the simulations is almost six times greater than in the experiments. Those differences might be attributed to differences in surface diffusion in experiment and simulation ( $T_S=RT$ , but  $D=300$ ).

### E. Honeycomb templated substrates: Influence of deposition angle

Figure 6 shows the morphological evolution of Si films grown on rapidly rotating ( $\rho \leq 105$  nm/rev) honeycomb templated substrates ( $s=419$  nm,  $h(\text{Au})=50$  nm) for different deposition angles  $\theta$ . The angle  $\theta$  was varied in four steps, besides the cases of on-axis deposition ( $\theta=0^\circ$ ) and GLAD ( $\theta=85^\circ$ ),  $\theta=35^\circ$  and  $\theta=70^\circ$  were chosen to span the range between the two extreme cases. The films with heights  $t$  between 430 and 540 nm show remarkable morphological

differences. For  $\theta=0^\circ$ , a continuous, dense film is obtained, with hillocks on top that resemble the honeycomb template of the substrate [Fig. 6(a)]. At  $\theta=35^\circ$ , the shadowing effect of the Au dots is still insufficient to remarkably shadow the interseed distances (for  $\theta=35^\circ$ , the shadowing length for a seed of height 50 nm equals approximately 30 nm), as can be seen in Fig. 6(b). Thus, a continuous film topped with honeycomblike arranged hillocks can still be found. At  $\theta=70^\circ$ , however, the effects of shadowing dominate the growth of the Si films, see Figs. 6(c). Instead of a closed film, an array of vertical nanorods growing on the Au dots is deposited. Unlike in the case of GLAD ( $\theta=85^\circ$ ), however, those rods are partially merged to each other, depending on the growth direction on the honeycomb pattern, and are intersected by a pyramidal-shaped layer that fills the space between the seeds and terminates growing at some stage. Finally, at  $\theta=85^\circ$ , the glancing angle case is fulfilled, and separated, rodlike nanostructures with triangular cross section in honeycomb arrangement are deposited.

In order to compare the experimental observations concerning the development of nanostructures on rapidly rotating honeycomblike patterned substrates with appropriate simulations, the following simulation parameters were chosen:  $s=70$  lu,  $h=15$  lu,  $\text{NPR}=1 \times 10^6$  (fast rotational speed), and  $\text{NOP}=1.5 \times 10^7$ . Just as in the experiment, the deposition angle  $\theta$  was varied in four steps between  $0^\circ$  and  $85^\circ$ . The results are shown in Figs. 6(e)–6(h).

At  $\theta=0^\circ$ , a continuous film that is topped with hillocks that replicate the templates' honeycomb arrangement is developing. At  $\theta=35^\circ$ , the bottom of the simulated film is still continuous and covered with features in honeycomb arrangement whose diameter is approximately twice the diameter of the hillocks that blanket the film simulated at  $\theta=0^\circ$ . At  $\theta=70^\circ$ , in good comparison to the experimental results, partially merged, broad, rodlike structures develop on the seeds and are intersected by pyramidal structures growing on the substrate surface between the artificial seeding spaces. For glancing angle conditions ( $\theta=85^\circ$ ), clearly separated rodlike structures that adopt the periodicity of the template pattern evolve in the simulations, with only little growth between the seeds.

At  $\theta=0^\circ$  and  $\theta=35^\circ$ , both experiments and simulations show the development of a continuous film that is capped with dots, arranged in a honeycomb pattern and replicating the Au dot matrix underlying the deposited film. No fanlike aggregation that is reported for deposition with parallel ballistic flux at  $\theta=0^\circ$  (Refs. 31 and 32) can be found here. This remarkable difference between thin films grown with parallel ballistic flux and the sputtered particle flux used in our experiments and simulations indicates that the angular distribution of the incoming particles plays an important role in thin film depositions on templated substrates. Evidently, the sputtered particle flux used here fosters the formation of a continuous layer, topped with hillocks over the initial Au dots. Although at  $\theta=30^\circ$ , both simulation and experiment still result in dense films capped with periodically arranged hillocks, the enhanced agglomeration of the Si particles at the Au dots (as compared to the case of  $\theta=0^\circ$ ) is reflected in the increased diameter  $b$  of the dots arranged atop the closed

film:  $b(\theta=0^\circ)=48\pm 6$  nm, in contrast to  $b(\theta=30^\circ)=126\pm 8$  nm. In the simulations [Figs. 6(e) and 6(f)], the film development at  $\theta=0^\circ$  and  $\theta=30^\circ$  is qualitatively the same as in the experimental observations, although a quantitative comparison is difficult, as for example the ratios  $h/s$  are not the same in experiment in simulation. Nevertheless, the development of continuous films that are capped with hillock features which are arranged just as the underlying template pattern for sputter deposition at low particle incoming angles is also shown in the simulations.

At  $\theta=70^\circ$ , the effect of shadowing becomes more dominant, favoring the agglomeration at the Au seeds and leading to the development of rodlike nanostructures that are intersected by pyramidal shaped structures between the Au seeds. Unlike in the glancing angle case ( $\theta=85^\circ$ ), however, those rods are partially merged to each other, depending on the growth direction on the honeycomb pattern. This behavior can be understood as follows. On a honeycomblike template pattern, the distances between the seeds are different in different directions. In Fig. 1(a), this is indicated with two different directions  $d_1$  and  $d_2$ . In direction  $d_1$ , the interseed distance is approximately 420 nm, whereas in direction  $d_2$ , alternating interseed distances of approximately 240 and 480 nm appear. For the case of a rotationally symmetric nanostructure grown by shadowing-efficient oblique angle deposition, the scaling prediction that the radius  $R$  of the nanostructure obeys a power law  $R\sim t^p$  (where  $p$  is the growth exponent) holds on both flat substrates<sup>19</sup> and artificially seeded substrates in square arrangements.<sup>9</sup> Additionally, in a previous work,<sup>9</sup> the independence of the growth exponent  $p$  of the interseed distance is predicted as well as the evolution of a saturation radius  $R_{\text{sat}}$  that scales with the interseed distance  $d$  according to a power law  $R_{\text{sat}}\sim d^q$ .

In the case of  $\theta=70^\circ$ , it is found that the radius  $R$  of the growing nanocolumns is not saturating. The structures increase their diameter with increasing height, until they eventually touch and merge together. Cross-sectional SEM micrographs of cuts along the directions  $d_1$  and  $d_2$  of Si films of total height  $t=1080$  nm reveal a merging of the structures at heights  $t$  that depend on the direction of the cut and, therefore, on the distance between the seeds in different directions [Figs. 7(a) and 7(b)]. However, until the onset of this merging behavior, the radius of the growing column increases according to a power law just as in the GLAD case well-described in literature. Along direction  $d_1$  (constant interseed distances of approximately 420 nm), the growth exponent  $p$  was determined from the plot of the  $R(t)$ -dependence ( $R$  values are averaged over six columns) to  $p=0.37\pm 0.04$  [Fig. 7(d)]. This is in good accordance to the  $p$  values predicted for the glancing angle case ( $\theta=85^\circ$ ) that are supposed to be in the range between  $0.30 < p < 0.50$ , depending on the strength of surface diffusion,<sup>19</sup> although a direct comparison is not possible due to the difference in the deposition angle. The growth exponent for other growth directions is difficult to obtain, since, for example, in direction  $d_2$  the alternating change of interseed distances leads to the a nonuniform broadening of the columns. If, however, we assume the growth exponent to be universal for every growth direction, it follows that the height  $t$  at which merging sets in is highly

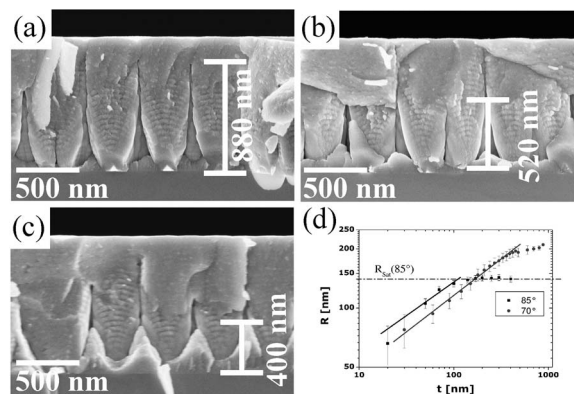


FIG. 7. Cross-sectional micrographs of GLAD Si films of total height  $t=1080$  nm deposited at  $\theta=70^\circ$  in different growth directions. (a) Direction  $d_1$ . (b) Direction  $d_2$ . (c) Pyramidal-shaped growth front of Si grown between the seeds of the honeycomb templates for  $\theta=70^\circ$ . (d) Relationship between structure radius  $R$  and film height  $t$  in direction  $d_1$  for  $\theta=70^\circ$  and  $\theta=85^\circ$ .

dependent on the distance between the seeds and therefore on the direction of growth. In direction  $d_1$  (constant interseed distance of approximately 420 nm), the merging starts at a film height of  $t\approx 880$  nm, see Fig. 7(a). In direction  $d_2$ , a merging of the columns grown on dots with nearest-neighbor distance 240 nm can be observed at  $t\approx 520$  nm, see Fig. 7(b). The ratio of the heights of beginning merging for different interseed distances,  $880/540$  nm = 1.62 is close to the ratio of those different interseed distances themselves, which is  $420/240$  nm = 1.75. Therefore, it is likely that the growth exponent is the same for every growth direction, which in turn leads to a faster merging in directions of less interseed distance. As the longest interseed distance is 480 nm (in direction  $d_2$ ), the merging of the structures sets in latest in this direction, leaving hcp-arranged open pores with pore diameters on the nanometer scale while the film around these hole is already closed [see, for example, inset of Fig. 6(i)]. The pyramidal-shaped interseed grown film at  $\theta=70^\circ$  [Fig. 7(c)] is a direct consequence of the reduced shadowing effect of the Au dots as compared to the case of  $\theta=85^\circ$ . At  $\theta=70^\circ$ , the shadowing length of the seeds is  $l\approx 137$  nm. Therefore, the radial space between six honeycomblike arranged Au dots is not completely shadowed, with the center of this circle gaining the most flux. As growth continues, the columns that grow on the Au seeds increase their diameter and gather most of the flux, which in turn is unable to reach the regions between the seeds any longer, until finally the growth of those interseed pyramids terminates.

Comparing the experiments with the simulated results at  $\theta=70^\circ$ , it can be seen that the principle features of the simulated film are in good accordance with the experimental results. As Figs. 6(g) and 6(j) show, oblique angle sputter deposition at rather large incoming angles on honeycomb templates results in rodlike nanostructures with different diameter evolutions in different growth directions. A nonuniform diameter evolution with film height due to different interseed distances in the growth direction  $d_2$  in the simulations can be seen, leading to an early merging for the structures growth fronts when the seed distances are small. Also, the pyramidal-shaped interseed-grown structures that are allocated to insufficient flux capturing by the seeds are clearly

visible in the simulations. Again, a more quantitative comparison of experimental and simulated results is difficult, as the dimensions of the used template systems cannot be directly compared.

At  $\theta=85^\circ$ , the shadowing length of the Au seeds is sufficient enough to shadow the whole region between the seeds ( $l \approx 570$  nm). In this case, vertical nanorods with a triangular cross section grow on the honeycomblike seed pattern [Fig. 6(d)]. The triangular cross section is again a consequence of the different interseed distances in different growth directions.<sup>16</sup> However, unlike in the case of  $\theta=70^\circ$ , the diameter of the columns saturates at a certain point, without merging together of the separated structures. Along direction  $d_1$ , the growth exponent is found to be  $p = 0.34 \pm 0.03$  and the saturation radius is  $R_{\text{sat}} \approx 135$  nm. The interseed growth is again attributed to nondirectional particle flux. Eventually, the same trends as in the experiments can be seen in the simulated deposition [Fig. 6(h)].

## V. CONCLUSIONS

In conclusion, we have shown both experimentally and with Monte Carlo simulations that the form, cross section, and periodicity of glancing angle sputter deposited nanostructures depend strongly on the substrate temperature (i.e., surface diffusion), type of substrate (unpatterned, patterned with different geometries and different seed heights), the ratio  $\rho$  of substrate rotational speed to deposition rate, and the deposition angle  $\theta$  of the incident sputtered particle flux.

Concerning the deposition of nanospirals at different substrate temperatures, recent results showing that the surface diffusion has a strong impact on merging behavior, single nanostructure diameter and overall density of the deposited film<sup>23</sup> could be extended with Monte Carlo simulations at different diffusion steps that clearly mirror the experimental results.

On templates with honeycomb arranged seeds, depending on  $\rho$  spirals, screws or rods can be grown in a periodically arrangement for sufficiently large seed heights. In the case of fast substrate rotation, it could be shown that different values of  $\theta$  ( $0^\circ$ ,  $35^\circ$ ,  $70^\circ$ , and  $85^\circ$ ) change the type of the deposited layer from a closed film capped with honeycomblike arranged hillocks (normal incidence) to a film consisting of nanostructures partially grown together in distinct directions and intersected by pyramids growing on the interseed regions (at  $\theta=70^\circ$ ) to separated, rodlike nanostructures with triangular cross sections ( $\theta=85^\circ$ ). The triangular cross section at  $\theta=85^\circ$  as well as the partial merging of structures in different growth directions at  $\theta=70^\circ$  was related to the assumption that the rod diameter obeys a scaling rule  $R \sim t^p$ ,<sup>19</sup> explaining a different growth saturation behavior in different growth directions on honeycomb templates. The growth ex-

ponents in the direction of equidistantly distributed seeds were found to be  $p=0.37 \pm 0.04$  for  $\theta=70^\circ$  and  $p = 0.34 \pm 0.03$  for  $\theta=85^\circ$ .

## ACKNOWLEDGMENTS

This work is supported by the project P3 within the DFG research group FOR 522 “Architecture of nano- and microdimensional structure elements.”

- <sup>1</sup>K. Robbie, L. J. Friedrich, S. K. Dew, T. Smy, and M. J. Brett, *J. Vac. Sci. Technol. A* **13**, 1032 (1995).
- <sup>2</sup>M. M. Hawkeye and M. J. Brett, *J. Vac. Sci. Technol.* **25**, 1317 (2007).
- <sup>3</sup>S. R. Kennedy, M. J. Brett, O. Toader, and S. John, *Nano Lett.* **2**, 59 (2002).
- <sup>4</sup>Q. H. Wu, L. de Silva, M. Arnold, I. J. Hodgkinson, and E. E. Takeuchi, *J. Appl. Phys.* **95**, 402 (2004).
- <sup>5</sup>J. J. Steele, A. C. van Popta, M. M. Hawkeye, J. C. Sit, and M. J. Brett, *Sens. Actuators B* **120**, 213 (2006).
- <sup>6</sup>S. V. Kesapragada, P. Victor, O. Nalamasu, and D. Gall, *Nano Lett.* **6**, 854 (2006).
- <sup>7</sup>M. Malac and R. F. Egerton, *Nanotechnology* **12**, 11 (2001).
- <sup>8</sup>B. Dick, M. J. Brett, T. Smy, M. Belov, and M. R. Freeman, *J. Vac. Sci. Technol. B* **19**, 1813 (2001).
- <sup>9</sup>E. Main, T. Karabacak, and T.-M. Lu, *J. Appl. Phys.* **95**, 4346 (2004).
- <sup>10</sup>D. X. Ye, T. Karabacak, B. K. Lim, G. C. Wang, and T. M. Lu, *Nanotechnology* **15**, 817 (2004).
- <sup>11</sup>E. Schubert, T. Höche, F. Frost, and B. Rauschenbach, *Appl. Phys. A: Mater. Sci. Process.* **81**, 481 (2005).
- <sup>12</sup>C. Patzig, B. Rauschenbach, W. Erfurth, and A. Milenin, *J. Vac. Sci. Technol. B* **25**, 833 (2007).
- <sup>13</sup>C. M. Zhou and D. Gall, *Appl. Phys. Lett.* **88**, 203117 (2006).
- <sup>14</sup>C. M. Zhou and D. Gall, *Thin Solid Films* **515**, 1223 (2006).
- <sup>15</sup>C. M. Zhou and D. Gall, *J. Vac. Sci. Technol. A* **25**, 312 (2007).
- <sup>16</sup>C. Patzig, B. Rauschenbach, B. Fuhrmann, and H. S. Leipner, *J. Appl. Phys.* **103**, 024313 (2008).
- <sup>17</sup>C. M. Zhou and D. Gall, *Appl. Phys. Lett.* **90**, 093103 (2007).
- <sup>18</sup>T. Karabacak, Y. P. Zhao, G. C. Wang, and T. M. Lu, *Phys. Rev. B* **64**, 085323 (2001).
- <sup>19</sup>T. Karabacak, J. P. Singh, Y.-P. Zhao, G.-C. Wang, and T.-M. Lu, *Phys. Rev. B* **68**, 125408 (2003).
- <sup>20</sup>D. X. Ye and T. M. Lu, *Phys. Rev. B* **76**, 235402 (2007).
- <sup>21</sup>J. J. Steele and M. J. Brett, *J. Mater. Sci. Mater. Electron.* **18**, 367 (2007).
- <sup>22</sup>M. Suzuki, K. Nagai, S. Kinoshita, K. Nakajima, K. Kimura, T. Okano, and K. Sasakawa, *Appl. Phys. Lett.* **89**, 133103 (2006).
- <sup>23</sup>C. Patzig and B. Rauschenbach, *J. Vac. Sci. Technol. A* **26**, 881 (2008).
- <sup>24</sup>T. Karabacak, G.-C. Wang, and T.-M. Lu, *J. Vac. Sci. Technol. A* **22**, 1778 (2004).
- <sup>25</sup>H. J. Qi, J. D. Shao, D. P. Zhang, K. Yi, and Z. X. Fan, *Appl. Surf. Sci.* **253**, 3004 (2007).
- <sup>26</sup>B. Fuhrmann, H. S. Leipner, H. R. Höche, L. Schubert, P. Werner, and U. Gösele, *Nano Lett.* **5**, 2524 (2005).
- <sup>27</sup>E. Schubert, J. Fahlteich, B. Rauschenbach, M. Schubert, M. Lorenz, M. Grundmann, and G. Wagner, *J. Appl. Phys.* **100**, 016107 (2006).
- <sup>28</sup>Image Metrology, [www.imagemet.com](http://www.imagemet.com).
- <sup>29</sup>T. Karabacak and T.-M. Lu, in *Handbook of Theoretical and Computational Nanotechnology*, edited by M. Reith and W. Schommers (American Scientific Publishers, Stevenson Ranch, CA, 2005), Chap. 69, p. 729.
- <sup>30</sup>A. Laktakhia and R. Messier, *Sculptured Thin Films: Nanoengineered Morphology and Optics* (SPIE, Bellingham, WA, 2005).
- <sup>31</sup>D.-X. Ye and T.-M. Lu, *Phys. Rev. B* **75**, 115420 (2007).
- <sup>32</sup>P. Ramanlal and L. M. Sander, *Phys. Rev. Lett.* **54**, 1828 (1985).